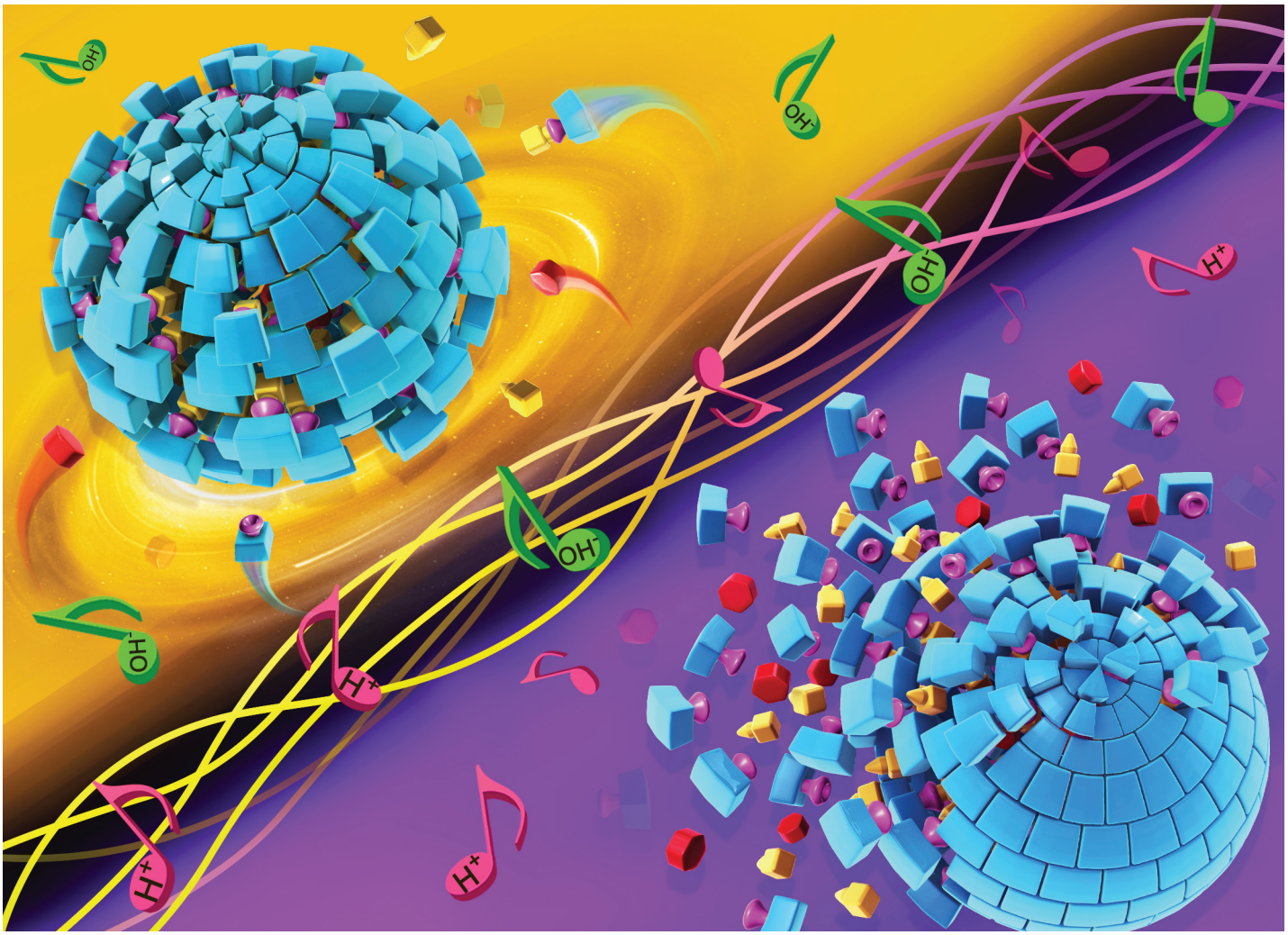

Showcasing research from Prof. Can Zhang and Prof. Tingjie Yin's group at China Pharmaceutical University, Nanjing, P. R. China.

Facile dynamic one-step modular assembly based on boronic acid-diol for construction of a micellar drug delivery system

This study reports a facile and dynamic one-step modular assembly strategy based on boronic acid-diol for constructing focus-responsive micellar drug delivery systems using hydrophobic, hydrophilic and the objective drug molecular building blocks. This newly proposed approach voids the tedious and tough procedures of the traditional construction approach based on covalently synthesized amphiphiles, and simultaneously exhibits promise in stimuli-responsive drug delivery. It opens a new sight for easy-to-assemble and disassemble drug delivery nano-vehicles.

As featured in:

See Tingjie Yin, Can Zhang *et al.*, *Biomater. Sci.*, 2018, **6**, 2605.

ROYAL SOCIETY OF CHEMISTRY

rsc.li/biomaterials-science

Registered charity number: 207890

Biomaterials Science

PAPER

View Article Online
View Journal | View Issue

Cite this: *Biomater. Sci.*, 2018, **6**, 2605

Facile dynamic one-step modular assembly based on boronic acid-diol for construction of a micellar drug delivery system†

Zekai Zhao,[a] Ying Zhang,[a] Chunli Tian,[a] Tingjie Yin *[b] and Can Zhang*[a]

Nano-assembled amphiphilic micelles with characteristics including facile control, a simplified construction procedure, convenient and efficient drug loading, and a controlled release at pathological sites are in high demand. This study reports a facile and dynamic one-step modular assembly strategy based on boronic acid-diol for constructing focus-responsive micellar drug delivery systems. In this manner, a dopamine modified hydrophilic building block, phenylboronic acid modified hydrophobic building block and drug molecules (Dox) spontaneously one-step assembled into drug encapsulated distinct core/shell micelles (Dox/PBAE-M) in mild physiological media. After a simple adjustment of weight ratios between these three building blocks, Dox/PBAE-M, with the highest Dox-loading capacity (22.4%) and optimal physical dimensions, was generated. Furthermore, the desirable pH-dependent disassembly of Dox/PBAE-M was independently verified by morphological changes alongside *in vitro* release of Dox in different simulated environments. The experimental results here demonstrated that Dox/PBAE-M kept structural integrity in normal physiological environments, while accomplishing a selective nano-disassembly and Dox release within acid endo/lysosomes. As a result, Dox/PBAE-M exhibited the highest cytotoxicity and apoptosis induction among all of the tested groups on the 4T1 breast cancer xenograft model. This newly proposed assembly strategy gave new insight into easy fabrication and disassembly of multi-functional micellar drug delivery systems.

Received 27th June 2018,
Accepted 19th July 2018

DOI: 10.1039/c8bm00712h

rsc.li/biomaterials-science

Introduction

Self-assembled polymeric micelles (PMs) are of widespread interest in pharmaceutical research, owing to their advantages which include their excellent abilities to solubilize hydrophobic drugs, and their good steric stabilities due to distinct core/shell structures.[1,2] Applying these PMs makes it possible for bioactive components to reach their objective sites, generating pharmacodynamic potency.

Recently, the compatibility and miscibility between the core-forming polymeric matrix and the solutes have been concluded to be the key points of micellar drug-loading efficiency and stability both *in vitro* and *in vivo*.[3,4] However, major PMs are constructed from conventional amphiphiles containing both hydrophobic and hydrophilic blocks covalently bonded together. As a result, scientific screening for an optimal block match is necessary to determine the amphiphile most compatible to specific drug molecules.[5,6] In this case, the chemical modification-associated complexity, un-controllability and the lack of structural flexibility has actually hindered the further clinical development of PMs.

Fortunately, modular assembly has emerged as a facile and straightforward strategy for constructing nanostructures.[7,8] In this manner, diverse materials are transformed into building blocks and further organized easily by intermolecular associations to form ordered assemblies, just like what we encounter with toy bricks. Consequently, application of modular amphiphilic assembly based on hydrophobic and hydrophilic building blocks in PMs' construction avoids tedious and tough procedures and overcomes the structural constraints of traditional polymeric assemblies.[9] Nevertheless, these modular assembly-based PMs might be faced with a general lack of controlled release function. Their drug release efficiency could be limited by the gradual degradation kinetics of nano-matrixes, which usually lead to sub-optimal drug potency.

[a]*State Key Laboratory of Natural Medicines and Jiangsu Key Laboratory of Drug Discovery for Metabolic Diseases, Center of Advanced Pharmaceuticals and Biomaterials, China Pharmaceutical University, Nanjing 210009, China. E-mail: zhangcan@cpu.edu.cn; Tel: +86 25 83271102*
[b]*State Key Laboratory of Natural Medicines, Department of Pharmaceutics, China Pharmaceutical University, 24 Tongjiaxiang, Nanjing 210009, China. E-mail: cookey_89ytj@163.com*

†Electronic supplementary information (ESI) available. See DOI: 10.1039/c8bm00712h

Therefore, we herein propose a dynamic one-step modular assembly strategy based on boronic acid-diol for the construction of drug-loaded PMs. Covalent coupling between the individually modified boronic acid and diol building blocks spontaneously and efficiently proceeds under mild physiological conditions, and is susceptible to acidity-triggered cleavage.[10–14] Moreover, it is worth noting that the drug loading performance following the construction of the PMs may not only complicate the preparation procedure, but also affect the structural stability of the original assemblies.[15,16] However, in our proposed strategy, the objective drug molecules can be conveniently loaded into the PMs through a one-step co-assembly with building blocks. Furthermore, the resulting micellar structure, drug-loading efficiency and particulate stability can be easily controlled by modulating the assembly process and the weight ratios between the drugs and the different building blocks. Collectively, the basic characteristics of modular assembly including good controllability, simplicity and structural tailorability,[8] plus its unique pH-dependent dynamic covalent functionality agree well with the objective manner for convenient construction of therapeutics-loaded PMs with the ability of controlled release.

As shown in Scheme 1, the model hydrophobic drug (adriamycin (Dox)), the diol modified hydrophilic building block (Poly-DA), and the boronic acid modified hydrophobic building block (PBA-DOCA) were simply dissolved together and in one step assembled into Dox-loaded core/shell micelles (Dox/PBAE-M) in neutral physiological environments. After reasonable regulation of the molar ratios between these three building blocks, DOX/PBAE-M, with the best amphiphilic equilibrium, and subsequent highest drug-loading and particulate stability, was conveniently generated.

In the following, the 4T1 breast cancer model was selected to evaluate the systemic drug delivery efficiency of PBAE-M constructed by the dynamic one-step modular assembly. After intravenous injection, the obtained Dox/PBAE-M were expected to be highly resistant to physiological destruction and remain stable in blood circulation, followed by accumulation at tumor sites through enhanced permeability and retention (EPR) effects. Once internalized into acidic endo/lysosomes, phenylboronate bonds would be quickly cleaved and initiate nano-disassembly. Dox/PBAE-M underwent acid-triggered de-stabilization, with notable Dox leakage during intracellular trafficking, thereby favoring nuclear accumulation and promoting the anticancer effect of Dox. PBAE-M validated the great promise of our newly proposed facile and dynamic one-step modular assembly strategy for easy fabrication of focus-responsive micellar drug delivery systems.

Experimental procedures

Materials

Doxorubicin hydrochloride (Dox·HCl) was bought from Huafeng United Technology Co., Ltd (Beijing, China). Phenylboronic acid (PBA), dopamine (DA) hydrochloride and deoxycholic acid (DOCA) were acquired from Energy Chemical Co., Ltd (Shanghai, China). Poly(isobutylene-*alt*-maleic anhydride) [poly(IB-*alt*-MAnh)], (M_w ~ 6000) was bought from Sigma-Aldrich Chemical Co., Ltd (Shanghai, China). Trypsin (Gibco) and RPMI1640 medium (1640, Gibco) were obtained from Pufei Biotechnology Co., Ltd (Shanghai, China). 3-(4,5-Dimethylthiazol-2-yl)-2,5-diphenyltetrazolium bromide (MTT), fetal bovine serum (FBS), and penicillin–streptomycin solution (Hyclone) were purchased from SunShine Biotechnology Co., Ltd (Nanjing, China). LysoTracker Green and the near-infrared dye DiR were obtained from Life Technologies (United States). All other chemicals and reagents were analytical grade.

Synthesis of building blocks for dynamic modular assembly and amphiphilic polymers for non-dynamic traditional assembly

Synthesis of hydrophobic building blocks: phenylboronic acid modified deoxycholic acid (PBA-DOCA). 1 g (1.00 eq.) of DOCA was dissolved in 100 mL of tetrahydrofuran (THF), followed by addition of 788.37 mg DCC (1.50 eq.) and 351.79 mg NHS (1.20 eq.). After 12 h of reaction at room temperature under a nitrogen atmosphere, the precipitated dicyclohexylurea was removed by filtration. Then, the filtrate was precipitated in *n*-hexane. The succinimido DOCA was filtered off, washed thoroughly with *n*-hexane and dried *in vacuo* at room temperature for 24 h.

Next, *N*-deoxycholyl ethylenediamine (DOCA-NH_2) was synthesized by introducing ethylenediamine to the succinimido DOCA. Briefly, succinimido DOCA was dissolved in DMF (5 mL), and the solution was added dropwise into 17 mL of ethylenediamine. After reaction for 6 h, the mixture was precipitated in *n*-hexane. The white powder DOCA-NH_2 was obtained with a yield of 95% after three washes with *n*-hexane and a further 24 h of drying at reduced pressure.

Finally, PBA-DOCA was synthesized through conjugating PBA with DOCA-NH_2. PBA (83.99 mg, 1.10 eq.), EDC (132.31 mg, 1.50 eq.) and NHS (63.55 mg, 1.20 eq.) were dissolved in 5 mL of DMF. After an addition of DOCA-NH_2 (200 mg), the mixture was stirred at room temperature for 24 h. Then, the mixture was precipitated in distilled water. The white precipitate was collected by filtration, followed by three washes with distilled water, and lyophilized. The product was finally purified by silica gel column chromatography. The molecular weight was detected by High Resolution Mass Spectrometer (HR-MS, JMS-800D). ^{1}H-NMR (d6-DMSO; 300 MHz; δ ppm): 8.82 (s, 1H, C_6H_4CONH); 8.05–7.52 (m, 5H, C_6H_4CONH); 4.62 (s, 1H, CHO*H*); 4.38 (s, 1H, CHO*H*); 4.17 (d, 2H, $B(OH)_2$); 3.77 (s, 2H, CH_2CH_2); 3.90–3.54 (d, 5H, $NHCH_2CH_2NH$ + C*H*OH); 0.91–0.56 (m, 12H, $CHCH_3$).

Synthesis of hydrophilic building blocks: dopamine conjugated polymers (Poly-DA). 311.71 mg (1.00 eq.) of poly(IB-*alt*-MAnh) and 300.00 mg (1.10 eq.) of dopamine were dissolved in 10 mL of DMF. After a further addition of 35.14 mg (0.20 eq.) of 4-dimethylaminopyridine (DMAP) and 0.59 mL (2.50 eq.) of *N*,*N*-Diisopropylethylamine (DIPEA), the mixture was reacted at room temperature for 24 h and dialyzed (3500

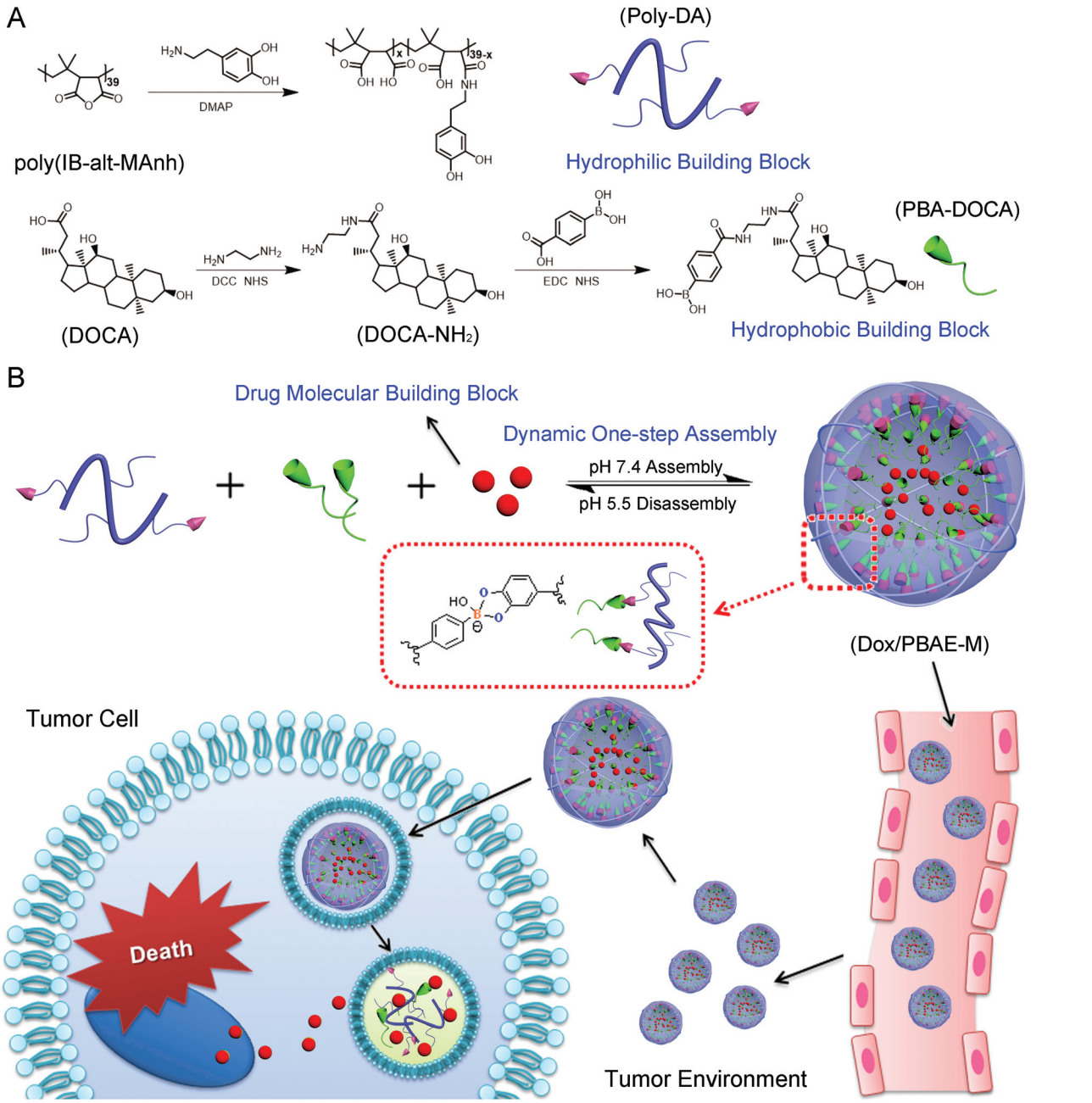

Scheme 1 (A) Preparation of hydrophobic and hydrophilic building blocks. (B) The dynamic one-step modular assembly of different building blocks to achieve the drug-loaded micelles, Dox/PBAE-M. Illustration of the tumor accumulation and the intracellular trafficking pathway of Dox/PBAE-M. The intracellular trafficking pathway includes steps of non-specific endocytosis, pH-triggered disassembly, Dox release and accumulation in the nucleus.

Da MWCO) under vacuum exhaustively. The final solution was lyophilized and Poly-DA was obtained at a yield of 89%. ^{1}H-NMR (D_2O; 300 MHz; δ ppm): 6.75–6.26 (d, 3H, C6H_3); 1.24–0.37 (d, 8H, CH_2(CH_3)$_2$).

Synthesis of deoxycholic acid modified poly(isobutylene-*alt*-MAnh), poly-DOCA, for non-reversible traditional assembly. 188.74 mg (0.20 eq.) of NH_2-DOCA and 400.00 mg (1.00 eq.) of poly (IB-*alt*-MAnh) were dissolved in 10 mL of DMF, followed by addition of 53.05 mg (0.20 eq.) of DMAP and 0.36 mL (1.00 eq.) of DIPEA. After stirring for 24 h, the mixture was precipitated in cold acetone. The precipitates were dissolved in water and dialyzed (MWCO of 3.5 kDa) for 48 h and then lyophilized to obtain a white semisolid with a yield of 97%. ^{1}H-NMR (d^6-DMSO + D_2O; 300 MHz; δ ppm): 7.48 (s, 2H, CON*H*CH$_2$CH$_2$N*H*CO); 4.19 (s, 1H, CHOH); 3.31 (s, 2H, CONHCH_2); 0.65 (s, 3H, C$H_{3(DOCA)}$).

pH-Dependent interactions between PBA and dopamine compounds. Phenylboronic acid (PBA) and dopamine (DA)

hydrogen chloride were dissolved in d^6-DMSO respectively to achieve the concentration of 0.2 M, followed by mixing together to obtain a stock solution of PBA-DA conjugate (0.1 M). After dilution by 0.1 M of monosodium phosphate D_2O solution, the pH of the obtained 1 mM PBA-DA solution was adjusted to 4.5, 5.5 and 7.4, respectively, using 10 N NaOH in D_2O. As a control, the PBA and DA were dissolved singly (0.1 M) in d^6-DMSO. Subsequently, the final solutions were analyzed by ^{1}H NMR spectra on a Bruker (AVACE) AV-500 spectrometer and the integrals of characteristic peaks in the range of 8.0 to 6.0 ppm were used for quantifying the degree of acid triggered dissociation of PBA-DA.

Alizarin red S (ARS) was used to characterize the binding efficiency between the PBA-DOCA and Poly-DA.[14] Briefly, different molar ratios of Poly-DA and PBA-DOCA were premixed in 1980 μL of a mixed solution containing PBS (10 mM, pH 7.4), DMF and DMSO at volume ratio of 1 : 6.6 : 8.24. ARS solution (5 mM, 20 μL) was then added into the above solutions and the corresponding fluorescence signals were measured by fluorescence spectrometry (RF-5301 PC, SHIMADZU) at an excitation wavelength of 468 nm.

Preparation and characterization of Dox-loaded micelles, Dox/PBAE-M and Dox/nPBAE-M

Preparation of Dox/PBAE-M and Dox/nPBAE-M. Dox/PBAE-M was prepared by a simple dialysis method based on a reversible one-step modular assembly. Firstly, the hydrophobic building block (PBA-DOCA), hydrophilic building block (Poly-DA) and the drug molecule (Dox) were dissolved in a mixed solution of DMSO (500 μL) and PBS (10 mM, pH 7.4, 100 μL) at different weight ratios. Then, the mixture was added into PBS (10 mM, pH 7.4, 3 mL) under stirring, and further dialyzed against PBS (10 mM, pH 7.4, 3 L) using a dialysis bag (MWCO = 3.5 kDa) for 24 h to remove free Dox molecules and DMSO. Finally, the resulting Dox/PBAE-M was obtained through filtration using a 0.45 μm millipore filter. As a non-reversible comparison, Dox/nPBAE-M was obtained following the same procedure described above, except using the mixed solution of Poly-DOCA and Dox instead of the mixture of PBA-DOCA, Poly-DA and Dox.

Physical characterization of Dox/PBAE-M and Dox/nPBAE-M. The particle size, polydispersity index (PDI) and zeta potential of Dox/PBAE-M and Dox/nPBAE-M were measured by dynamic light scattering (DLS) using a Malvern Zetasizer Nano-ZS90 (Malvern Instruments, U.K.). The morphology of the micelles was examined using a transmission electron microscope (TEM, H-7650, Hitachi). Samples in TEM analysis were negatively stained with 0.1% phosphotungstic acid. The amount of Dox in the micelles was determined using a microplate reader. Dox/PBAE-M and Dox/nPBAE-M were diluted in DMSO, and the fluorescence intensity was measured at ex 503 nm, em 554 nm using a microplate reader (Infinite M200 PRO, Tecan). The drug-loading capacity (DL%) was calculated by the following formula:

$$\mathrm{DL}\% = W_{\mathrm{drug}}/(W_{\mathrm{drug}} + W_{\mathrm{carrier}}) \times 100\%,$$

where W_{drug} and W_{carrier} are the amounts of Dox and total building blocks in the resulting micelles, respectively.

pH-Dependent dynamic assembly of Dox/PBAE-M. To explore the pH-dependent dynamic assembly in the construction of Dox/PBAE-M, the particle size of the Dox-loaded micelles was measured after incubation with different buffer solutions including PBS (10 mM, pH 7.4), glucose supplemented PBS (10 mM, pH 7.4) and 10% FBS, NaAc/HAc (10 mM, pH 5.5) for different times. After dilution by these buffer solutions, the samples were incubated in a shaker at 37 °C at 100 rpm. The particle size and PDI of these samples were determined using DLS. The acid-triggered disassembly of Dox/PBAE-M after incubation in NaAc/HAc (10 mM, pH 5.5) for 12 h was further monitored by TEM imaging.

Dynamic assembly-based controlled drug release

The dialysis method was employed to investigate the *in vitro* Dox release behavior from Dox/PBAE-M and Dox/nPBAE-M. Briefly, 400 μL of Dox/PBAE-M or Dox/nPBAE-M containing 40 μg of Dox were added into the dialysis bag (MWCO 14 kDa) immersed in 40 mL of buffer solutions at different pH (7.4, 6.8, 5.5). All of the samples were placed in a shaker at 37 °C at 100 rpm. At predetermined time points (1, 2, 4, 8, 12, and 24 h), a 1 mL aliquot of the release medium was withdrawn and an equal volume of fresh medium was added. The amount of Dox released was assayed using the microplate reader.

Cell culture

4T1 cells, obtained from Cell Bank of Chinese Academy of Sciences (Shanghai, China), were cultivated in a complete 1640 medium with 100 μg mL^{-1} streptomycin and 100 U mL^{-1} penicillin at 37 °C under a 5% CO_2 atmosphere and at 90% relative humidity. The cells were sub-cultivated approximately every 2 days at a split ratio of 1 : 3.

Cellular uptake of Dox/PBAE-M and intracellular Dox release

4T1 cells at a density of 1×10^5 cell per well were seeded and cultured in 24-well plates for 48 h. The cells were incubated with different drug-loaded micelles for different times at 37 °C. After washing twice with cold PBS, 160 mL of cell lysis buffer (Beyotime, China) was added into each well and further incubated for 30 min. The BCA protein assay kit (Thermo Scientific) was used for quantifying the protein amount, while the drug concentration was measured by the microplate reader. The cellular uptake ($Q_{\mathrm{drug}}/Q_{\mathrm{protein}}$) efficiency was calculated, where Q_{drug} and Q_{protein} are the quantities of Dox in the cells and cell protein, respectively. To demonstrate the concentration-dependent uptake, different preparations with a Dox concentration in the range of 0.25–25 μg mL^{-1} were added into the given cell wells for 2 h of incubation. The following procedure was performed as the above described method to calculate the Dox uptake amount.

To estimate the endocytosis pathways of the Dox/PBAE-M, the cells were first cultured with various endocytosis inhibitors including 154 μg mL^{-1} of sucrose (inhibitor of clathrin-mediated endocytosis), 15 μg mL^{-1} of nystatin (inhibitor of

caveolin-mediated endocytosis), and 133 μg mL^{-1} of amiloride (inhibitor of macropinocytosis), respectively, for 1 h at 37 °C. Subsequently, an uptake study was performed in the presence of the above agents and different Dox-loaded micelles at a Dox concentration of 2.5 μg mL^{-1} for 4 h at 37 °C.[17,18] The next procedure to determine the intracellular amount of Dox was followed as described above in the cellular uptake study.

Next, a confocal laser scanning microscope (CLSM) was used to intuitively observe the acid-triggered intracellular Dox release. 4T1 cells (1×10^5 cells per well) were cultured in glass bottom dishes for 24 h. Then, different preparations containing 2.5 μg mL^{-1} of Dox were added for 2 h of incubation. After two washes by cold PBS, fresh 1640 medium, without FBS or Dox-loaded micelles, was incubated with the cells for another 0, 4 or 22 h. Finally, the cells were stained using 10 μg mL^{-1} of Hoechst 33342 (Beyotime Biotechnology, China) for 15 min and 1 mM of Lyso-Tracker Green (Beyotime Biotechnology, China) for 30 min. The intracellular Dox distribution was investigated using CLSM (LSM 700, Zeiss).

Cytotoxicity and cell apoptosis assay

The cytotoxicity of PBAE-M, nPBAE-M, Dox/PBAE-M and Dox/nPBAE-M was estimated using the 3-(4,5-dimethylthiazol-2-yl)-2,5-diphenyltetrazolium bromide (MTT) assay. 4T1 cells planted in 96-well plates at 1×10^4 cells per well were cultured for 24 h. Next, the cells were exposed to fresh 1640 medium containing different formulations at various Dox or polymer concentrations for 48 h. Afterwards, 20 μL of the MTT solution (5 mg mL^{-1}) was added into each well and incubated for 4 h. Then, the dark blue formazan crystals were dissolved with 150 μL of DMSO after discarding the supernatant. The UV absorbance intensity at 570 nm was determined by a microplate reader (Thermo Electron Corporation, USA).

The Annexin V-FITC/PI Apoptosis Detection Kit (Vazyme Biotech, Nanjing) was used for detection of 4T1 cell apoptosis. The cells planted in 6-well plates at 1×10^5 cells per well were cultured for 24 h. Then, the medium containing different preparations at a Dox concentration of 2.5 μg mL^{-1} was incubated with the cells for 48 h. In the following, the processing and staining of cell samples were conducted according to the manufacturer's protocol. Finally, the samples were analyzed using flow cytometry (BD AccuriC6, USA).

Animals and tumor xenograft models

The BaLB/c mice (18–25 g) were obtained from the Veterinary College of Yangzhou University (Jiangsu, China). All of the

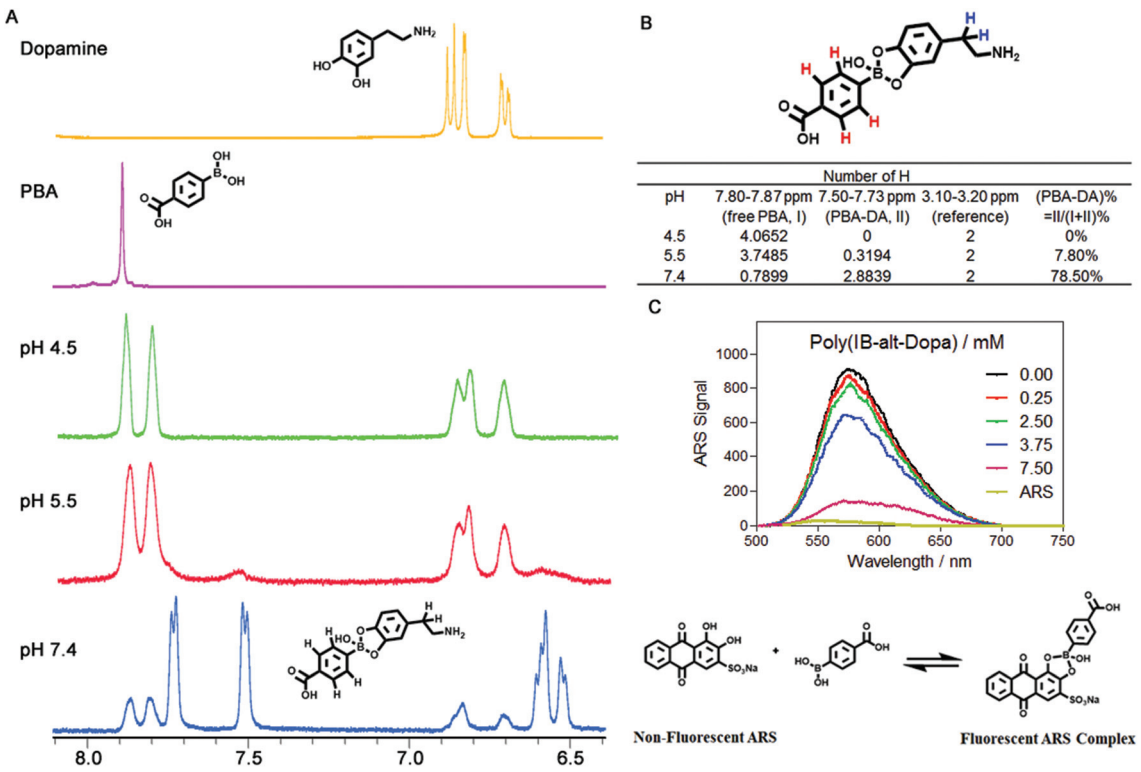

Fig. 1 (A) Characterization of the pH-dependent construction of phenylboronic acid-dopamine conjugate (PBA-DA) by ^{1}H-NMR. (B) Calculation of the binding degree between PBA and DA based on peak integrals from the obtained ^{1}H-NMR spectra at different pH. The peaks between 3.10 ppm and 3.20 ppm corresponded to H atoms on the methylene of DA (highlighted in blue, not shown in ^{1}H-NMR spectra); the peaks between 7.80–7.87 ppm represented H atoms on the phenyl ring of PBA (highlighted in red). In the PBA-DA conjugates, the H atoms on the phenyl ring of PBA shifted to the range of 7.50–7.73 ppm. (C) The fluorescence spectra of ARS (0.05 mM) after being added into the solutions containing PBA-DOCA (0.25 mM) at different molar ratios of Poly-DA (0–7.5 mM).

animal experiments were conducted under the relevant laws and followed the institutional guidelines of the China Pharmaceutical University. The China Pharmaceutical University institutional committee approved the experiments. The nude mice were subcutaneously inoculated in the armpit region with 4T1 cells (5×10^6 cells per mouse). The tumor volume (V) was measured by a vernier caliper and calculated as $V = a \times b^2/2$, where a was the largest diameter and b was the smallest.

Biodistribution

A non-invasive *in vivo* imaging technique was used to explore the biodistribution of PBAE-M in the 4T1 tumor bearing mice. DiR was loaded into PBAE-M and nPBAE-M in accordance with the method for loading Dox, and the DiR-loaded micelles DiR/PBAE-M and DiR/nPBAE-M were obtained. The BALB/c nude mice bearing 4T1 tumors around 200 mm^3 were injected with DiR/PBAE-M, DiR/nPBAE-M and free DiR intravenously at a DiR dose of 200 μg kg^{-1}. At predefined time points, the mice were anesthetized and imaged using Maestro *in vivo* imaging instruments (Cri Inc., USA). 24 h post injection, the main organs and tumors were harvested from the euthanized mice for *ex vivo* imaging. All of the images were analyzed using the Kodak Molecular Imaging Software 5.X.

In vivo antitumor efficacy

The tumor-bearing mice were weighed and randomly divided into different groups when the tumor volume reached 50 mm^3. From Day 0, the mice were intravenously injected with Dox solution (2 mg kg^{-1}), Dox/PBAE-M (2 mg kg^{-1}), Dox/nPBAE-M (2 mg kg^{-1}) or saline every other day.[19] The body weight and tumor size were recorded. After 14 days' observation, the mice were euthanized, the tumors and the normal organs (hearts, livers, spleens, lungs, and kidneys) were collected, washed with saline three times and fixed in 10% neutral-buffered formalin for histological evaluation by hematoxylin and eosin (HE) staining. The HE slices were observed through an optical microscope (Olympus, Japan).

Statistical analysis

The statistic of mean ± SD was appropriate and applicable to the results and one-way ANOVA or a two-tailed Student's t-test was used to test the statistical significance. A value of $P < 0.05$ was considered statistically significant.

Results and discussion

pH-Dependent interactions between phenylboronic acid (PBA) and dopamine (DA)

The pH-dependent dynamic binding between PBA and DA was firstly characterized using ^{1}H-NMR spectroscopy.[20] The PBA-DA constructed in d^6-DMSO was diluted by deuterated phosphate buffer to different pH (4.5, 5.5, and 7.4) and analyzed by ^{1}H-NMR. As exhibited in Fig. 1A, the mixture of PBA and DA at pH 4.5 possessed a spectrum similar to the superimposed one of the two individual compounds, indicating the presence of uncomplexed PBA and DA. In contrast, the spectrum of the same mixture at pH 7.4 exhibited notable changes in chemical shifts and peak splittings. Specifically, the Hs on the phenyl ring of PBA (Fig. 1B, highlighted in red) shifted from 7.80–7.87 ppm to the range of 7.50–7.73 ppm, while those of DA shifted from 6.70–6.85 ppm to the range of 6.53–6.58 ppm, which suggested the formation of PBA-DA conjugates based on phenyl borate bonds.

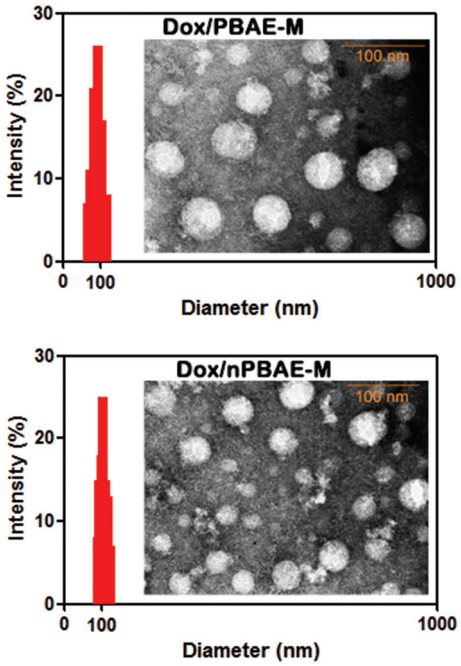

Fig. 2 The hydrodynamic size of Dox/PBAE-M and Dox/nPBAE-M measured by DLS. Inset: A TEM image of Dox/PBAE-M and Dox/nPBAE-M.

Table 1 Size, zeta potential and loading capacity of PBAE-M and nPBAE-M micelles (n = 3)

	m(PBA-DOCA) : m(Poly-DA) : m(Dox)[a]	Diameter (nm) (μ_2/Γ^2)	Zeta potential (mV)	DL (wt%)
Dox/PBAE-M	1 : 7 : 5	220.2 ± 2.3	−11.99 ± 2.23	5.2 ± 0.88
Dox/PBAE-M	2 : 7 : 5	120.3 ± 2.3	−9.45 ± 1.24	11.5 ± 2.38
Dox/PBAE-M	3 : 7 : 5	87.2 ± 0.9	−7.99 ± 2.03	22.4 ± 2.34
Dox/PBAE-M	4 : 7 : 5	135.9 ± 3.1	−7.12 ± 1.48	19.2 ± 3.17
Dox/PBAE-M	5 : 7 : 5	Precipitated	—	—
Dox/nPBAE-M	3 : 7 : 5	89.7 ± 0.9	−22.53 ± 2.71	26.6 ± 3.21

[a] The weight ratios of different building blocks (PBA-DOCA, Poly-DA and Dox).

Furthermore, the pH-dependent binding efficiency to form PBA-DA was quantitatively calculated according to the ratio between the peak integrals at 7.50–7.73 ppm (corresponding to the H amounts on the phenyl ring of PBA in PBA-DA conjugate) and the summed ones at 7.50–7.73 ppm and 7.80–7.87 ppm (corresponding to the H amounts on the phenyl ring of free PBA). As depicted in Fig. 1B, the binding efficiency between PBA and DA increased as the pH increased from 5.5 to 7.4, and the characteristic peaks of the phenyl borate bonds at 7.50–7.73 ppm were undetectable at pH 4.5. This result not only confirmed the pH dependence of the binding between PBA and DA, but also suggested that the PBA-contained building blocks and the DA-contained building blocks would successfully construct pH-responsive amphiphiles for drug delivery.

pH-Dependent dynamic one-step assembly between poly-DA and PBA-DOCA

Subsequently, the PBA-containing hydrophobic building blocks, PBA-DOCA, and the hydrophilic DA-containing building blocks, poly-DA, were synthesized following the procedure summarized in Scheme 1 and structurally identified by ^{1}H-NMR and HR-MS (Experimental section, Fig. S1–S3†). ARS exhibits superior binding ability with PBA.[14] Moreover, a dramatic increase in the fluorescence intensity of ARS appears upon binding with the PBA to form esters (Fig. 1C). Consequently, the efficiency of the assembly between PBA-DOCA and Poly-DA was evaluated through the competitive substitution of Poly-DA to ARS in phenylboronate bonding in aqueous solution. The resulting fluorescence intensity of ARS (0.05 mM) shown in Fig. 1C gradually declined with increasing amounts of Poly-DA (0–7.5 mM) introduced into the ARS/PBA-DOCA system. This result demonstrated that the ARS was successfully extricated from the ARS/PBA-DOCA complexes due to the binding efficiency between PBA-DOCA and Poly-DA.

The above demonstrated effective coupling of PBA-DOCA to Poly-DA was expected to mediate a facile one-step assembly with the Dox molecules to obtain drug-loaded core/shell micelles, Dox/PBAE-M. As depicted in Table 1, Dox/PBAE-M achieved an optimal physical dimension of 87.2 nm, and the

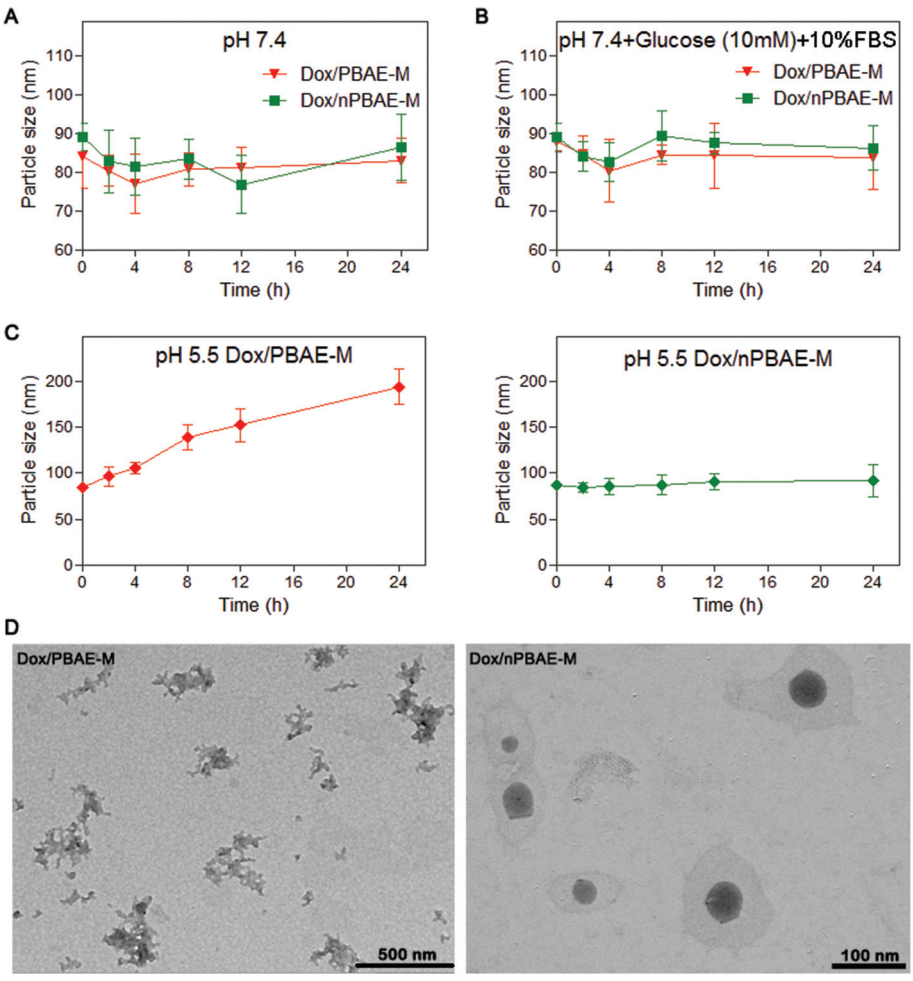

Fig. 3 The hydrodynamic size of Dox/PBAE-M and Dox/nPBAE-M measured by DLS after incubation at different conditions over time: (A) pH 7.4, (B) pH 7.4 + 10 mM glucose + 10% FBS, and (C) pH 5.5. (D) A TEM image of Dox/PBAE-M and Dox/nPBAE-M after incubation at pH 5.5 for 12 h.

highest drug-loading of 22.4% after a convenient screening of the weight ratios of different building blocks (PBA-DOCA, Poly-DA and Dox). The traditional micelles Dox/nPBAE-M which were assembled from the amphiphiles Poly-DOCA (structurally demonstrated by ^{1}H NMR in the Experimental section, Fig. S4†) were also prepared at the same feeding ratio as a comparison. Dox/nPBAE-M demonstrated similar physiochemical properties compared to the Dox/PBAE-M. Finally, the spherical morphology with uniform size distributions (below 100 nm) of the two Dox-loaded micelles was confirmed by transmission electron microscope (TEM) imaging (Fig. 2).

To further illustrate the pH-dependency of this facile one-step assembly strategy, a measurement by DLS was performed to monitor the size alterations of the Dox/PBAE-M in response to various simulated environments over 24 h. As exhibited in Fig. 3A and B, no significant change in size distribution was observed in the Dox/PBAE-M or Dox/nPBAE-M when exposed to pH 7.4 buffer solutions with 10 mM of glucose and 10% FBS, which corresponds to the physiological environment in blood circulation.[14] In contrast, Dox/PBAE-M showed a notable increase in particle diameter (Fig. 3C), specifically from 90.0 nm to 194.2 nm, when incubated in pH 5.5 buffer solutions for 24 h. Such a notable acid-triggered size increase in Dox/PBAE-M was mainly attributed to the phenylboronate linkages, and cleavage-mediated disassembly of micelles. The acid-triggered structural destruction of Dox/PBAE-M was also intuitively demonstrated through TEM imaging (Fig. 3D). In contrast, no significant change in size distribution and a maintained smooth core/shell structure was observed in Dox/nPBAE-M owing to the absence of the phenylboronate bonds. Overall, the data herein suggest that the Dox/PBAE-M constructed by the facile and dynamic one-step assembly strategy would retain structural integrity in blood circulation, but experienced pH-triggered disassembly within the acidic environments of endo/lysosomes. This finding validated the suitability of PBAE-M for efficient, specific, intracellular drug delivery.

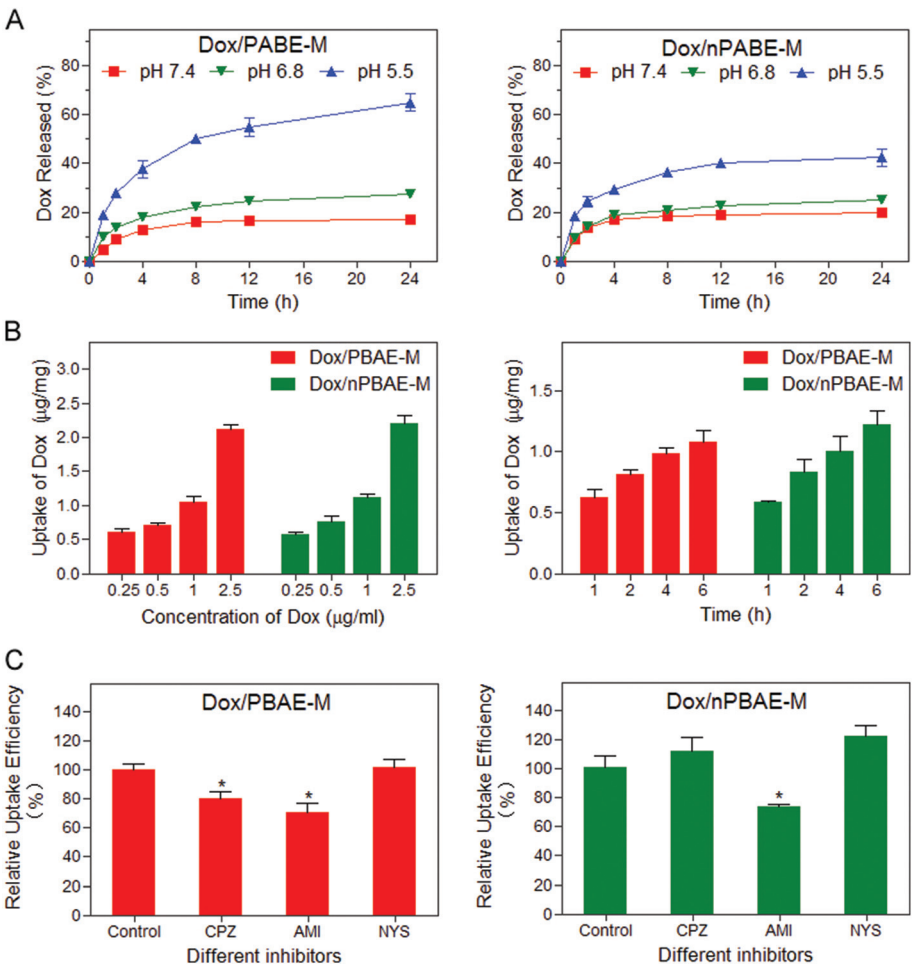

Fig. 4 (A) *In vitro* Dox release profiles of Dox/PBAE-M and Dox/nPBAE-M at different pH (7.4, 6.8, and 5.5) over time. (B) Cellular uptake of Dox/PBAE-M and Dox/nPBAE-M into 4T1 cells at various Dox concentrations for 2 h or at different time intervals with 2.5 μg mL^{-1} of Dox. (C) Relative uptake efficiency of Dox/PBAE-M and Dox/nPBAE-M in the presence of various endocytosis inhibitors. Data shown represent the mean ± SD (n = 5). *P < 0.05 *vs.* control.

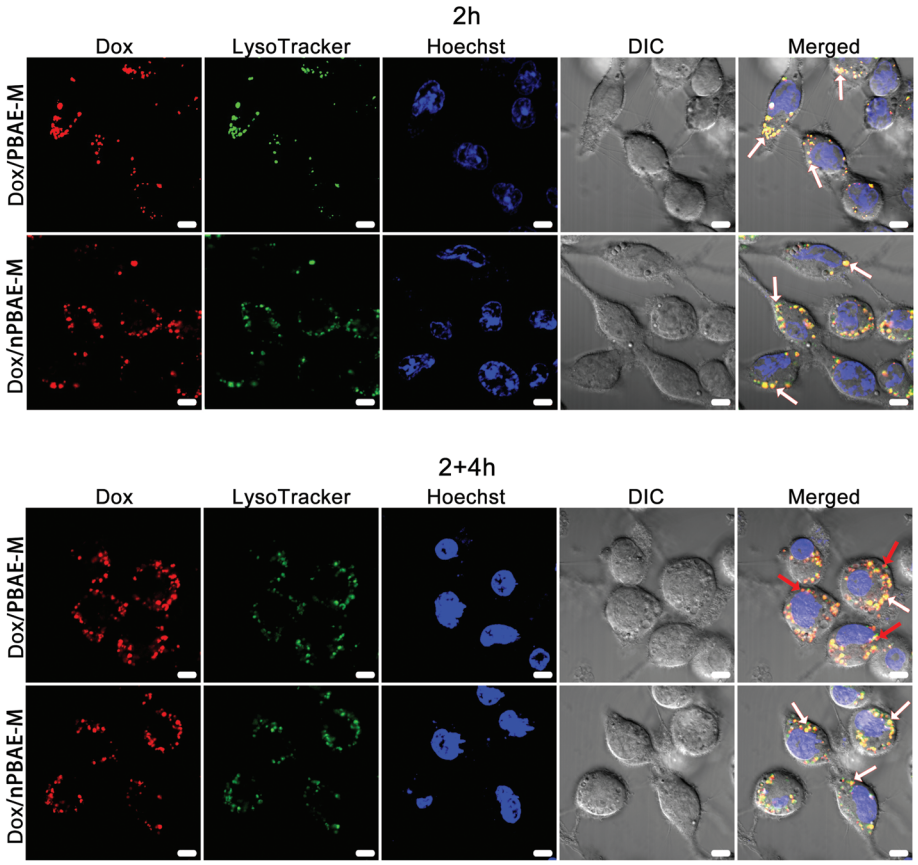

Fig. 5 CLSM images of the 4T1 cells for intracellular delivery of Dox by Dox/PBAE-M and Dox/nPBAE-M at different times. The late endosomes and lysosomes were stained by LysoTracker™ Green, and the nuclei were stained by Hoechst 33342. 2 + 4 h: incubation with Dox-loaded micelles for 2 h, followed by washing and further incubation for 4 h. White arrows indicate the overlap of yellow fluorescence of Dox and endo/lysosomes. Red arrows indicate the diffused red fluorescence of Dox. Scale bars are 5 μm.

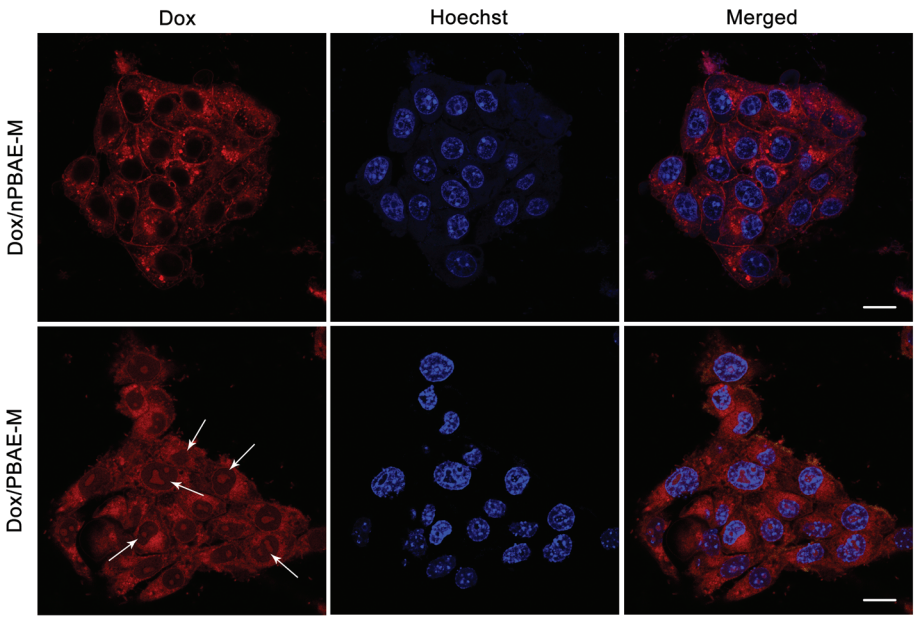

Fig. 6 Intracellular distribution of Dox/PBAE-M and Dox/nPBAE-M in 4T1 cells. The cells were incubated with Dox/PBAE-M or Dox/nPBAE-M for 2 h, and further incubated with fresh culture medium for an additional 22 h after removal of the excess micelles. The nuclei were stained by Hoechst 33342. Scale bars are 10 μm.

Dynamic assembly-based *in vitro* drug release

Next, to confirm the enhanced Dox release triggered by a cellular acid stimulus, we investigated *in vitro* Dox release profiles of Dox/PBAE-M in buffer solutions at different pH (7.4, 6.8, and 5.5). As exhibited in Fig. 4A, Dox/PBAE-M presented a pH-dependent drug release with greater release rates at lower pH values. Firstly, the Dox release from both Dox/PBAE-M and Dox/nPBAE-M was inefficient in simulated environments of blood circulation (pH 7.4) or tumor stroma (pH 6.8), and only around 20% of the Dox was released in 24 h. This result clarified that unintended extracellular Dox release could be kept to a minimum, decreasing potential systemic adverse effects. In contrast, in a buffer solution at pH 5.5, corresponding to the acid environment within intracellular endo/lysosomes, the release of Dox from Dox/PBAE-M was dramatically accelerated. Specifically, about 60% of the Dox was released in 24 h. However, less than 40% of the Dox was released from Dox/nPBAE-M which was irreversibly assembled from conventional amphiphiles after incubation at pH 5.5 for 24 h. The improved hydrophilicity of protonated Dox at pH 5.5 contributed to its slightly increased release rate over those at pH 7.4 and 6.8. Collectively, the dynamic assembly-based PBAE-M would tightly encapsulate Dox to minimize drug leakage during tumor extracellular transport, while achieving burst Dox release upon exposure to the intracellular specific acid microenvironment within endo/lysosomes.

Cellular uptake mechanisms, intracellular pH-triggered disassembly and Dox release from Dox/PBAE-M

Our next investigation centered around the cellular uptake efficiency and mechanism, as well as the reversible assembly-based intracellular Dox release. To assess this, the mouse breast adenocarcinoma cell line 4T1 was first incubated with Dox/PBAE-M and Dox/nPBAE-M at various Dox concentrations, or for different time intervals, followed by quantitatively detecting the cellular uptake efficiency of Dox (Fig. 4B). As depicted, Dox was delivered into 4T1 cells by Dox/PBAE-M and Dox/nPBAE-M in a Dox concentration- and time- dependent manner. Meanwhile, no significant distinction on the cell uptake was observed between dynamic and non-dynamically assembled micelles, which might be explained by the similarity of their nano-structures. Uptake studies on the 4T1 cells were further performed in the presence of chlorpromazine (CPZ), amiloride (AMI), or nystatin (CYS) which inhibited clathrin-mediated endocytosis, macropinocytosis, or caveolin-mediated endocytosis, respectively.[17,19,21] As shown in Fig. 4C, CPZ and AMI significantly decreased the cellular internalization of Dox/PBAE-M into 4T1 cells, while the uptake of Dox/nPBAE-M was remarkably decreased by AMI. This finding implied that macropinocytosis and clathrin were both involved in the 4T1 cellular uptake of Dox/PBAE-M, while the Dox/nPBAE-M is permeated into 4T1 cells mainly *via* macropinocytosis. However, both clathrin-mediated endocytosis and

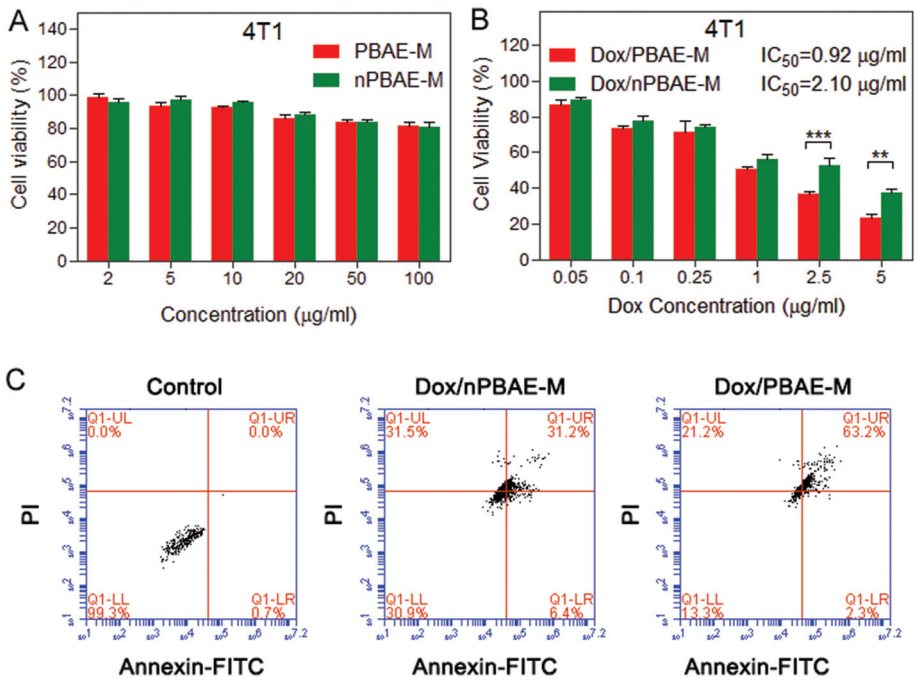

Fig. 7 *In vitro* cytotoxicity of (A) different drug loaded micelles or (B) blank micelles on the 4T1 cells for 24 h. The data were mean ± SD (n = 4). $^{**}P < 0.01$ *vs.* Dox/PBAE-M, $^{***}P < 0.001$ *vs.* Dox/PBAE-M. (C) Flow cytometric analysis of 4T1 cell apoptosis induced by Dox/PBAE-M and Dox/nPBAE-M for 48 h using the Annexin V-FITC/PI staining. In each panel, the lower-left (Annexin V-FITC$^-$, PI$^-$), lower-right (Annexin V-FITC$^+$, PI$^-$) and upper-right (Annexin V-FITC$^+$, PI$^+$) quadrants represent the populations of live cells, early apoptotic cells and late apoptotic cells, respectively. The average population (%) in each quadrant is indicated by the numbers at the corner of the panels.

macropinocytosis would transport Dox-loaded micelles into endo/lysosomes with low pH environments.[22–24]

Subsequently, the pH-triggered release and distribution of Dox by PBAE-M was intuitively demonstrated using confocal laser scanning microscopy (CLSM). The 4T1 cells were incubated with Dox/PBAE-M and Dox/nPBAE-M for 2 h, followed by thorough washing, and further incubated with fresh culture medium for 4 h or 22 h. As indicated by the white arrows in Fig. 5, colocalization of red labeled Dox/PBAE-M or Dox/nPBAE-M with green labeled endo/lysosomes generated a yellow overlay after the first 2 h of incubation. This result confirmed that most of the Dox-loaded micelles were firstly transported into the endo/lysosomes, which was in line with results from the above studies for the cellular uptake mechanisms. However, after an additional 4 h of incubation, a higher Dox fluorescence intensity and a more conspicuous dissociation of the red-labeled Dox from the green-labeled endo/lysosomes were observed in Dox/PBAE-M over pH non-sensitive Dox/nPBAE-M, demonstrating the acid-trigger disassembly and thus accelerated Dox delivery by PBAE-M. Moreover, as the time extended to 22 h, the obtained magenta fluorescence shown in Fig. 6 illustrated that the released Dox from Dox/PBAE-M subsequently accumulated in nuclei, eliciting drug potency. In all, the dynamically assembled PBAE-M allows efficient drug transport to the tumor cells mainly *via* an acid endo/lysosomal pathway, followed by pH-triggered effective

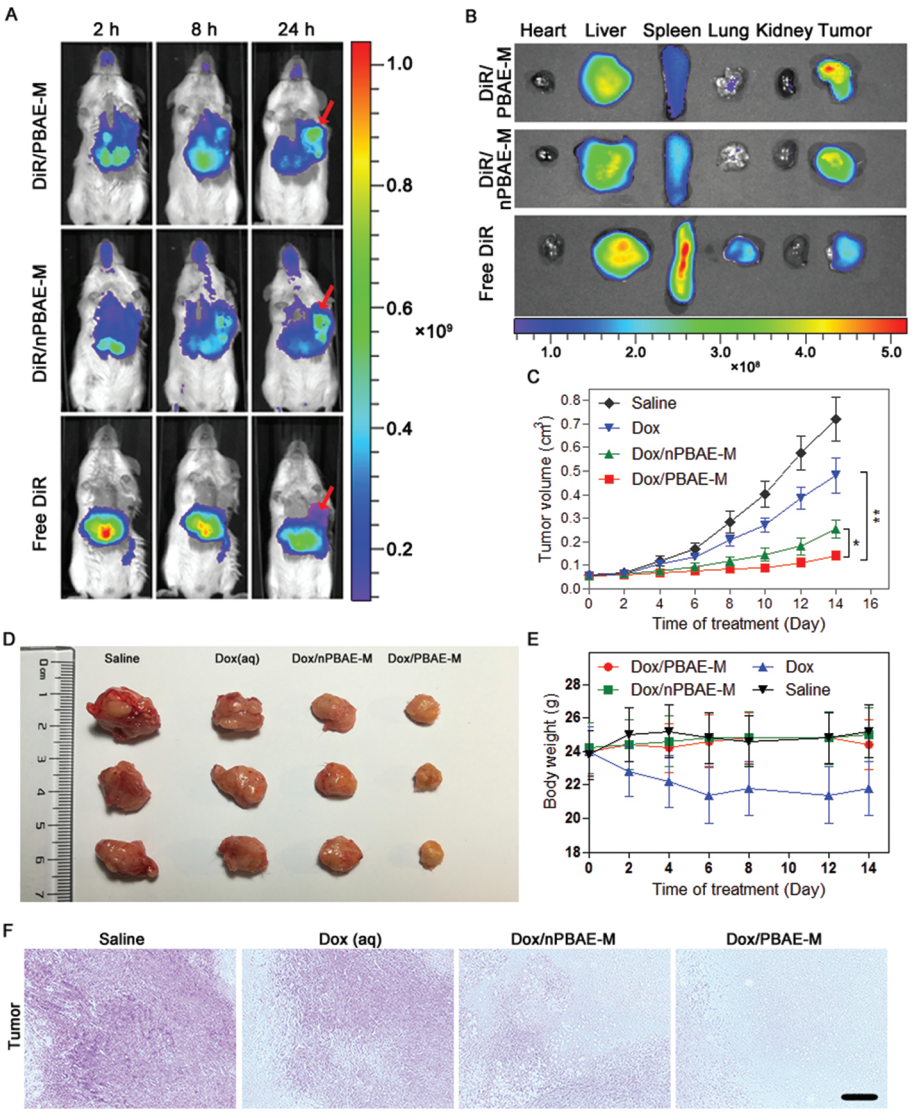

Fig. 8 (A) *In vivo* fluorescence imaging of the 4T1 tumor-bearing mice at 2, 8 and 24 h after intravenous injection of DiR/PBAE-M, DiR/nPBAE-M and free DiR at a dose of 0.2 mg kg^{-1}. Arrows indicate the sites of the tumors. (B) *Ex vivo* fluorescence imaging of the tumor and normal tissues harvested from the euthanized 4T1 tumor-bearing mice at 24 h post injection. (C) Tumor growth inhibition of the 4T1 tumor-bearing mice after multiple injections of different Dox formulations. The data represent the means ± S.D. (n = 5, $^{**}P < 0.01$, $^{*}P < 0.05$) (D) *Ex vivo* tumor images at the last day of *in vivo* treatment. (E) Body weight changes of 4T1 tumor-bearing mice treated with various formulations. (F) Histological observation of the tumor tissues after treatment using H&E staining. The scale bar is 100 μm.

disassembly and drug liberation favoring pharmacological responses.

Dox-induced cell apoptosis and cytotoxicity

To identify whether the facile and dynamic assembly strategy-mediated rapid drug delivery could favor pharmacological responses, the *in vitro* cytotoxicity of Dox/PBAE-M against the 4T1 cells was evaluated by an MTT assay with Dox/nPBAE-M as comparison. The results in Fig. 7A indicate that bare PBAE-M and nPBAE-M exhibit negligible toxicities on the 4T1 cells with a cell viability larger than 90%, even at concentrations as high as 100 μg mL^{-1}. The Dox/PBAE-M presented a significantly enhanced cytotoxicity compared with the Dox/nPBAE-M towards 4T1 cells at a Dox concentration of 2.5 μg mL^{-1} ($P < 0.001$) and 5 μg mL^{-1} ($P < 0.01$). The corresponding half-maximal inhibitory concentration (IC_{50}) of Dox/PBAE-M was 0.92 μg mL^{-1}. This value was 2.28-fold lower than that of Dox/nPBAE-M, which was mainly attributed to the dynamically assembly-mediated rapid DOX release. Furthermore, the observed enhancement in antitumor efficacy by Dox/PBAE-M was also verified through an Annexin V-FITC/PI detection assay. As illustrated in Fig. 7B, the Dox/PBAE-M induced a significantly higher total apoptotic ratio (65.5%) compared with Dox/nPBAE-M (37.6%). In summary, the more efficient intracellular Dox release from Dox/PBAE-M over Dox/nPBAE-M enhanced the pharmacological therapy towards cancer cells.

Tumor targeting and antitumor efficiency

To determine the systemic tumor targeting ability of the PBAE-M, the biodistribution of DiR-loaded micelles, DiR/PBAE-M, was tested on the 4T1 tumor bearing mice utilizing noninvasive near infrared optical imaging (Fig. 8A). Most of the DiR in DiR/PBAE-M and DiR/nPBAE-M accumulated in the liver and tumor 2 h post injection. As time progressed, a preferential accumulation of DiR fluorescence signals were found in tumor sites over the normal tissues 24 h after administration. In contrast, the free DiR group exhibited a major distribution of DiR in the liver and no notable tumor accumulation was observed even at 24 h post injection. These results provided decisive evidence for the EPR-based tumor targeting effect of both micelle platforms. 24 h after injection, mice were euthanized and tissues were excised for *ex vivo* imaging (Fig. 8B). As depicted, the DiR signal in the tumor site of the DiR/PBAE-M was comparable to that of the DiR/nPBAE-M, but much higher over that of the corresponding normal tissues. However, the DiR was mainly distributed in the liver and spleen when administrated in free molecular styles. Overall, the PBAE-M based on the facile and dynamic assembly was resistant to physiological destruction during blood circulation, and can serve as a highly efficient tumor-targeted delivery vehicle based on a passive targeting mechanism.

The following investigation sought to estimate the antitumor efficacy of Dox/PBAE-M in 4T1 tumor xenograft models.

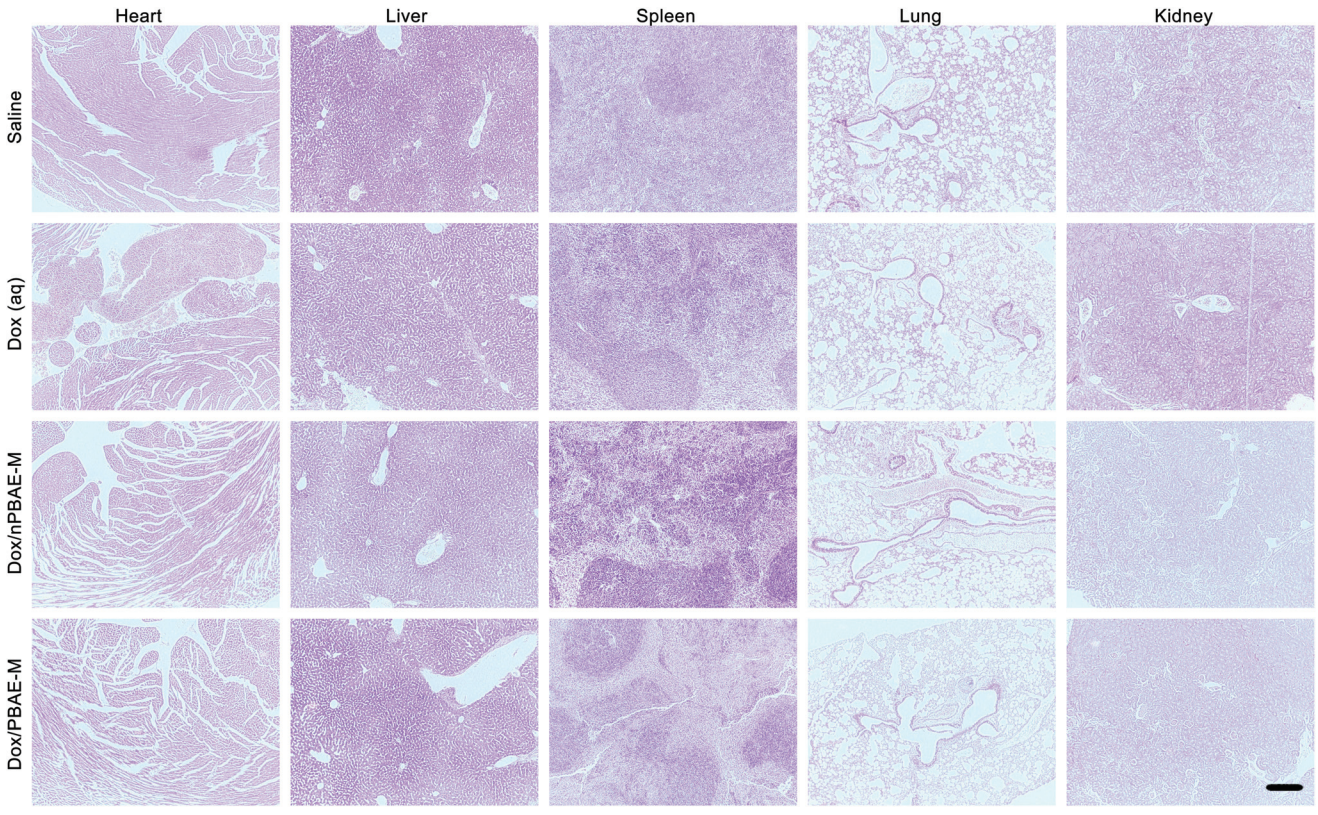

Fig. 9 Histological observation of the normal organs after treatment using H&E staining. The scale bar is 100 μm.

As shown in Fig. 8C and D, all of the Dox formulations demonstrated notable effects on inhibiting tumor growth compared with saline as a negative control. Both Dox/nPBAE-M and Dox/PBAE-M generated a remarkably higher inhibition efficacy towards tumor growth than the Dox·HCl solution, mainly attributed to the lack of the tumor targeting of Dox·HCl. Moreover, Dox/PBAE-M outperformed all of the other tested platforms including Dox/nPBAE-M in tumor-size inhibition, directly suggesting the advantages of this controllable and dynamically assembled nano-platform. The body weights of mice exhibited no noticeable change during the treatment with Dox/PBAE-M and Dox/nPBAE-M (Fig. 8E). However, a significant body weight decrease was observed after the treatment of Dox·HCl, which resulted from the severe adverse effects of the non-selectively distributed Dox. Afterward, the histologic images of tissue sectioning using H&E staining displayed a massive cancer cell remission after treatment with Dox/PBAE-M (Fig. 8F), while exhibiting no obvious pathological abnormalities in normal organs (Fig. 9), such as cardiomyopathy in the heart induced by the Dox treatment. The pH-dependent self-assembled PBAE-M was verified to firmly encapsulate and transport hydrophobic drugs to tumors, demonstrate effective intracellular internalization and pH-accelerated drug release, and as a result achieved an optimal *in vivo* anticancer efficacy with negligible side effects.

Conclusions

In this study, we developed a facile and dynamic one-step modular assembly strategy based on boronic acid-diol for construction of drug-loaded micelles using hydrophobic, hydrophilic and the objective drug molecular building blocks. The modal drug-loaded micelles, Dox/PBAE-M, were conveniently obtained with controlled micellar structure, drug-loading efficiency and particulate stability after a simple modulation of the weight ratios between the different building blocks. Moreover, Dox/PBAE-M was verified to retain a stable micellar structure and firmly encapsulate therapeutics under normal physiological conditions, while disassembling once internalized into acid endo/lysosomes in a targeted disease focus for a promoted drug release, thus achieving an enhanced therapeutic efficiency. This newly proposed approach avoids the tedious and tough procedures of the traditional construction approach based on covalently synthesized amphiphiles, and simultaneously exhibits promise in stimuli-responsive drug delivery. It opened new insight into easy assembly and disassembly of drug delivery nanovehicles.

Conflicts of interest

There are no conflicts to declare.

Acknowledgements

This work was supported by the National Natural Science Foundation of China (81773664, 81473153, 81703442), the National Basic Research Program of China (2015CB755504), the 111 Project from the Ministry of Education of China and the State Administration of Foreign Expert Affairs of China (No. 111-2-07). The authors thank the public platform of State Key Laboratory of Natural Medicines for assistance with Confocal Microscopy and Flow Cytometry.

References

1 H. Chen, W. Zhang, G. Zhu, J. Xie and X. Chen, *Nat. Rev. Mater.*, 2017, **2**, 17024–17054.
2 P. Couvreur, *Adv. Drug Delivery Rev.*, 2013, **65**(1), 21–23.
3 S. Kim, Y. Shi, J. Y. Kim, K. Park and J. X. Cheng, *Expert Opin. Drug Delivery*, 2010, **7**, 49–62.
4 Y. Zhao, F. Fay, S. Hak, J. M. Perez-Aguilar, B. L. Sanchez-Gaytan, B. Goode, R. Duivenvoorden, D. Lange Davies, A. Bjørkøy, H. Weinstein, Z. A. Fayad, C. Pérez-Medina and W. J. M. Mulder, *Nat. Commun.*, 2016, **7**, 11221–11232.
5 J. Liu, Y. Xiao and C. Allen, *J. Pharm. Sci.*, 2004, **93**, 132–143.
6 K. Letchford, R. Liggins and H. Burt, *J. Pharm. Sci.*, 2008, **97**, 1179–1190.
7 M. J. Webber, E. A. Appel, E. W. Meijer and R. Langer, *Nat. Mater.*, 2016, **15**(1), 13–26.
8 J. L. Guo, B. L. Tardy, A. J. Christofferson, Y. L. Dai, J. J. Richardson, W. Zhu, M. Hu, Y. Ju, J. W. Cui, R. R. Dagastine and I. Yarovsky, *Nat. Nanotechnol.*, 2016, **11**(12), 1105–1113.
9 C. Wang, Z. Wang and X. Zhang, *Acc. Chem. Res.*, 2012, **45**(4), 608–618.
10 J. Zhu, S. Wan, D. Zheng, Q. Lei, R. Zhuo, J. Feng and X. Zhang, *ACS Appl. Mater. Interfaces*, 2017, **9**(1), 255–265.
11 Y. Kubo, R. Nishiyabu and T. D. James, *Chem. Commun.*, 2015, **51**(11), 2005–2020.
12 Y. Wang, Z. Chai, L. Ma, C. Shi, T. Shen and J. Song, *RSC Adv.*, 2014, **4**, 53877–53884.
13 R. Nishiyabu, Y. Kubo, T. D. James and J. S. Fossey, *Chem. Commun.*, 2011, **47**, 1124–1150.
14 Y. Li, W. Xiao, K. Xiao, L. Berti, J. Luo, H. P. Tseng, G. Fung and K. S. Lam, *Angew. Chem., Int. Ed.*, 2012, **51**(12), 2864–2869.
15 S. May and A. Fahr, *Drug Delivery Strategies for Poorly Water-Soluble Drugs*, John Wiley & Sons Ltd, 2013, ch. 1, pp. 1–35.
16 N. Ahmed, C. E. Mora-Huertas, C. Jaafar-Maalej, H. Fessi and A. Elaissari, *Drug Delivery Strategies for Poorly Water-Soluble Drugs*, John Wiley & Sons Ltd., 2013, ch. 5, pp. 151–197.
17 Q. Sun, Z. Kang, L. Xue, Y. Shang, Z. Su, H. Sun, Q. Ping, R. Mo and C. Zhang, *J. Am. Chem. Soc.*, 2015, **137**(18), 6000–6010.
18 A. G. Assanhou, W. Li, L. Zhang, L. Xue, L. Kong, H. Sun, R. Mo and C. Zhang, *Biomaterials*, 2015, **73**, 284–295.

19 R. Mo, T. Jiang, R. DiSanto, W. Tai and Z. Gu, *Nat. Commun.*, 2014, **5**, 3364–3374.
20 J. Su, F. Chen, V. L. Cryns and P. B. Messersmith, *J. Am. Chem. Soc.*, 2011, **133**(31), 11850–11853.
21 R. Mo, Q. Sun, N. Li and C. Zhang, *Biomaterials*, 2013, **34**(11), 2773–2786.
22 R. S. Flannagan, V. Jaumouillé and S. Grinstein, *Annu. Rev. Pathol.*, 2012, **7**, 61–98.
23 G. Scita and P. P. Di Fiore, *Nature*, 2010, **463**(7280), 464–473.
24 S. Mayor and R. E. Pagano, *Nat. Rev. Mol. Cell Biol.*, 2007, **8**(8), 603–612.

